Experimental observation of invisibility to a broadband electromagnetic pulse by a cloak using transformation media based on inductor-capacitor networks

Chao Li, Xiao Liu, and Fang Li

Institute of Electronics, Chinese Academy of Sciences, No. 19, North 4th Ring Road West, Haidian District, Beijing 100190, China

(Received 20 October 2009; revised manuscript received 8 January 2010; published 22 March 2010)

Invisibility devices have captured the imagination of humankind throughout the ages. In this paper, the response of a cylindrical cloak to a broadband electromagnetic (EM) pulse was experimentally investigated. The transformation medium of the cloak devices was realized with full parameters based on a nonuniform inductor-capacitor (L-C) network. Based on the experiment and simulation results, the time delay effect, the pulse broadening effect, and the scattered energy reduction ability of the cloak were studied. The dynamic process of the pulse propagating across the cloak device was also measured. It is found that the nonresonant nature of the unit cell structures leads to the low dispersion of the cloak parameters and results in the invisibility of the cloak to the broadband EM pulse. The broadband property of the proposed cloak may offer more practical applications in reducing the scattering of an object.

DOI: 10.1103/PhysRevB.81.115133 PACS number(s): 41.20.Jb, 42.25.Fx, 42.25.Gy, 42.79.−e

I. INTRODUCTION

The methods to make objects invisible to electromagnetic (EM) radiations have always been a subject of keen interest in microwave and optical society. Various schemes have been proposed to achieve invisibility, such as scattering cancellation with plasmonic shells,[1,2] anomalous localized resonance,[3,4] and invisible cloaks based on transformation optics.[5–20] Of special interest is the transformation approach because the proposed invisibility devices are not sensitive to the size, composition and geometry of the objects being concealed. The basic principle of the idea is to squeeze a volume in a virtual space into a shell with complex material parameters in the physical space based on the invariance transformation of Maxwell's equations.[5–7] Recent research progress of artificial metamaterials (MTMs) with flexible and tunable EM parameters offers a possible way to realize these kinds of complex devices. However, it is still a nontrivial thing when it comes to realization because the required material parameters for such cloaks are not only anisotropic, but also spatially inhomogeneous. So far, most of the researches on invisibility cloaks have been limited to theoretical analysis and numerical simulations.[7–17]

The first experimental demonstration[6] was conducted at microwave frequencies using metallic ring MTMs with varied magnetic resonances to achieve a set of simplified constituent parameters, which inevitably lose part of the cloaking effect. And the inherent resonances of the metallic rings naturally result in strong dispersion and limit the device to a very narrow frequency range. Latterly, a nonmagnetic version of partial cloak, with reduced parameters which only approximates the radial component of the dielectric permittivity, was studied experimentally in the visible frequency range.[18] Obviously, it is still a partial cloak and can only reduce the visibility of an object to some extent even in theory. Recently, "carpet cloaks" employing nonresonant elements were both proposed in the microwave[19] and infrared.[20] Although in this scheme the bandwidth can be extended to a wider range, the objects could only be concealed in the region between the carpet cloak and a conducting sheet in the reflection mode. This considerably limits the potential of the cloaks. A transmission-line (TL) method has also been proposed to design cloak device under a different concept which does not employ the transformation optics.[21] The drawback of this method is that the shape and the size of the object to be cloaked must fits inside the space between the adjacent sections of the TLs in the cloaked region. This inevitably leads to the difficulty for cloaking a bulky object. Lately, the authors have proposed a nonuniform inductor-capacitor (L-C) network method to model the cylindrical cloaks with full parameters based on the transformation optics,[22] and experimentally studied the performance of the device under stable states at different harmonic frequencies.[23]

In realistic applications, the dynamic responses of a cloak to a wideband time-domain signal is ultra important. In this paper, we experimentally demonstrated the invisibility of a cylindrical cloak to a broadband EM pulse. As proposed in Ref. 22, the cloak was designed based on a nonuniform L-C network with full parameters, in which the three branches of the inductor-capacitor (L-C) unit cells were employed to independently tuning each functional component of the anisotropic material tensors in the cylindrical basis. The reminder of paper is organized as follows: in Sec. II, the introduction of the key procedure for the cloak design method is given at first. Then the realization of the cloak device for experiment is presented. In Sec. III, the response of the cloak device to a broadband EM pulse is experimentally investigated. The time evolution of the narrow pulse in each node of the cloak device is measured using a network analyzer. Based on experiment and simulation results, the time delay effect, the pulse broadening effect, and the scattered energy reduction ability of the cloak were studied. The experimental results for the propagation of the pulse across the cloak device are dynamically shown. Due to the nonresonant nature of the unit cell structure, the low dispersion of the material parameters can be achieved which results in the broadband characteristic of the proposed cloak. Sec. IV gives some conclusions.

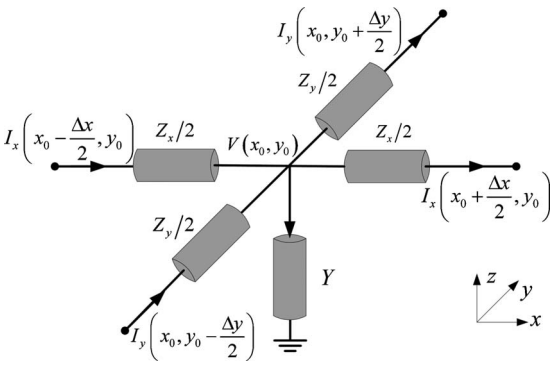

FIG. 1. The unit cell of a 2D TL network

II. DESIGN AND REALIZATION OF A CYLINDRICAL CLOAK WITH A NONUNIFORM L-C NETWORK

From the EM theory and the TL theory, media with specific permittivity and permeability can be modeled by L-C networks. The TL versions of isotropic right-handed materials (RHMs) and left-handed materials (LHMs) have been investigated several years ago[24,25] and been proposed to experimentally demonstrate the point-to-point focusing which overcomes the classical diffraction limit.[26,27] Additionally, Balmain *et al.* utilized 2D TL approach to synthesize planar anisotropic MTMs that exhibit sharp beams called "resonance cones"—a resonant phenomenon that takes place in anisotropic plasmas.[28] To our best knowledge, all the previously reported anisotropic TL MTMs have permittivity and permeability tensors diagonalized in the Cartesian basis, with unit cells uniformly repeated in cubic lattice. However, the medium parameters of an invisibility cloak are inhomogeneous and anisotropic with principle axes varying point to point. In our recent Letter paper,[22] a method was proposed to model full parameter cloaks by nonuniform L-C networks aligned in cylindrical lattice. In this section, the key procedure of the method will be introduced. Then, the realization of the cloak device for experiment will be presented.

Assuming a general case of a two-dimensional (2D) network with its unit cell schematically shown in Fig. 1, one can get following relations by applying Kirchhoff's voltage and current laws to the adjacent unit cells:

$$V(x_0,y_0) - V(x_0+\Delta x,y_0) = Z_x I_x\left(x_0+\frac{\Delta x}{2},y_0\right), \tag{1a}$$

$$V(x_0,y_0) - V(x_0,y_0+\Delta y) = Z_y I_y\left(x_0,y_0+\frac{\Delta y}{2}\right), \tag{1b}$$

$$\left[I_x\left(x_0-\frac{\Delta x}{2},y_0\right) - I_x\left(x_0+\frac{\Delta x}{2},y_0\right)\right] + \left[I_y\left(x_0,y_0-\frac{\Delta y}{2}\right) - I_y\left(x_0,y_0+\frac{\Delta y}{2}\right)\right] = YV(x_0,y_0), \tag{1c}$$

where Δx and Δy describe the dimension of the unit cell along x and y directions, respectively. For a cylindrical cloak, the permittivity and permeability tensors are simultaneously diagonalized in cylindrical basis. In this case, we can write the Maxwell's equations with differential form in cylindrical coordinates as following:

$$\frac{E_z(r+\Delta r,\theta) - E_z(r,\theta)}{\Delta r} = j\omega\mu_\theta H_\theta\left(r+\frac{\Delta r}{2},\theta\right), \tag{2a}$$

$$\frac{E_z(r,\theta+\Delta\theta) - E_z(r,\theta)}{r\Delta\theta} = -j\omega\mu_r H_r\left(r,\theta+\frac{\Delta\theta}{2}\right), \tag{2b}$$

$$\frac{\left(r+\frac{\Delta r}{2}\right)H_\theta\left(r+\frac{\Delta r}{2},\theta\right) - \left(r-\frac{\Delta r}{2}\right)H_\theta\left(r-\frac{\Delta r}{2},\theta\right)}{\Delta r} - \frac{H_r\left(r,\theta+\frac{\Delta\theta}{2}\right) - H_r\left(r,\theta-\frac{\Delta\theta}{2}\right)}{\Delta\theta} = j\omega r\varepsilon_z E_z(r,\theta). \tag{2c}$$

Here, TE mode is presumed with electric field polarized in z direction. Equations (1) and (2) can be mapped to each other with following replacements:

$$\Delta y \leftrightarrow r\Delta\theta, \quad \Delta x \leftrightarrow \Delta r, \quad I_y \leftrightarrow \Delta r H_r, \quad I_x \leftrightarrow -r\Delta\theta H_\theta,$$

$$V \leftrightarrow E_z d, \tag{3}$$

where d represents the cloak thickness along z direction. Then, the natures of the impedances and the admittances in Fig. 1 are also evident with following expressions:

$$Z_y = j\omega\mu_r d\frac{r\Delta\theta}{\Delta r}, \quad Z_x = j\omega\mu_\theta d\frac{\Delta r}{r\Delta\theta}, \quad Y = \frac{j\omega r\Delta\theta\Delta r\varepsilon_z}{d}, \tag{4a}$$

$$\omega r\Delta\theta\sqrt{\mu_r\varepsilon_z} = r\Delta\theta\sqrt{-Z_y\frac{\Delta r}{r\Delta\theta}\frac{Y}{r\Delta\theta\Delta r}} = \sqrt{-Z_yY} \ll 1, \tag{4b}$$

$$\omega\Delta r\sqrt{\mu_\theta\varepsilon_z} = \Delta r\sqrt{-Z_x\frac{r\Delta\theta}{\Delta r}\frac{Y}{r\Delta\theta\Delta r}} = \sqrt{-Z_xY} \ll 1. \tag{4c}$$

This means an inhomogeneous and anisotropic medium with permittivity and permeability diagonalized in cylindrical basis can be artificially synthesized by nonperiodic TL networks. The long-wavelength approximation has to be satisfied, where the dimension of the unit cell is much smaller than the wavelength.

As proposed in Ref. 7, a cylindrical cloak with inner radius a and outer radius b has the following radius-dependent, anisotropic permittivity and permeability:

$$\mu_r = \mu_b\frac{r-a}{r}, \quad \mu_\theta = \mu_b\frac{r}{r-a}, \quad \varepsilon_z = \varepsilon_b\left(\frac{b}{b-a}\right)^2\frac{r-a}{r}, \tag{5}$$

where ε_b and μ_b represent the permittivity and permeability of the background medium. Now, we consider the realization of the above material specification through an L-C network.

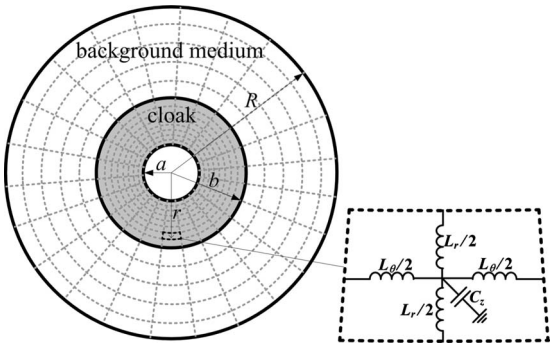

FIG. 2. The schematic show of the cloak shell and the background medium based on a L-C MTMs network

In each unit cell, μ_r, μ_θ, and ε_z are represented by two series inductance L_θ, L_r and one shunt capacitance C_z, respectively. Since the medium parameters of the cloak are radius-dependent, we can synthesize the whole cloak structure with concentric layers. Each layer consists of identical unit cells repeated along the angular direction. The schematic show of the cloak design using an L-C network is illustrated in Fig. 2. According to Eqs. (4) and (5), the relationship between the circuit parameters and the medium parameters of the cloak can be derived as

$$L_\theta(n) = \mu_b \frac{\Delta\theta_n}{\Delta r_n}(r_n - a)d, \quad L_r(n) = \frac{\mu_b}{r_n - a}\frac{\Delta r_n}{\Delta\theta_n}d,$$

$$C_z(n) = \varepsilon_b\left(\frac{b}{b-a}\right)^2 \frac{(r_n - a)\Delta r_n \Delta\theta_n}{d}, \tag{6}$$

where the subscription n represents the n^{th} layer, and r_n, Δr_n, $\Delta\theta_n$ represent the radial distance, the thickness and the span angle of the unit cell in the n^{th} layer, respectively.

In reality, the cloak should be connected to the real background medium, such as the free space, in a way like embedded in a parallel plate waveguide. For the sake of convenience in experiment, here the background medium is also mimicked by the conformal L-C network as shown in Fig. 2. Then, all the field distribution, in and outside the cloak shell, can be extracted by measuring the voltages in each node of the TL network. This does not lose the generality of our later experimental results. The circuit parameters for the unit cells in the n^{th} layer of the background medium can be derived based on Eq. (4) by substituting $\mu_r = \mu_\theta = \mu_b$, and $\varepsilon_z = \varepsilon_b$,

$$L_\theta(n) = \mu_b \frac{r_n \Delta\theta_n}{\Delta r_n}d, \quad L_r(n) = \mu_b \frac{\Delta r_n}{r_n \Delta\theta_n}d,$$

$$C_z(n) = \frac{\varepsilon_b r_n \Delta\theta_n \Delta r_n}{d}. \tag{7}$$

In our design, the outer boundary of the background medium is truncated at radius R by being connected with Bloch impedances,[29] which are applied to achieve match absorption and to mimic the infinite extended background.

Now, we consider the following implementation of the cloak based on the proposed method in this paper. The design frequency is chosen as 40 MHz, which is far below the

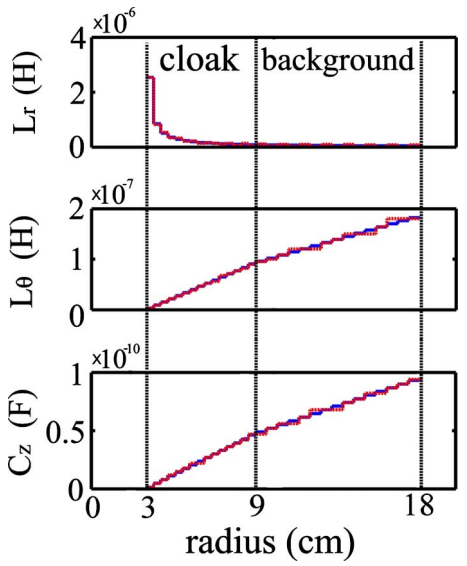

FIG. 3. (Color online) The theoretical and the experimental values of the lumped L-C elements along the radius direction. The blue solid line is for theoretical result and the red dotted line is for experimental result.

parasitic resonant frequencies of the lumped capacitors and inductors. To obtain a reasonable dimension of the whole structure including the cloak shell and the background, here we choose the permittivity and the permeability of the background medium as $\varepsilon_b = 10^{-3}\varepsilon_0$ and $\mu_b = 10^7\mu_0$, where ε_0 and μ_0 are the constitutive parameters of free space. The inner and outer radius of the cloak shell are chosen as $a=3$ cm and $b=9$ cm, respectively, and the truncated outer boundary of the background area has a radius $R=18$ cm. The network is fabricated by mounting chip capacitors and inductors on a FR-4 substrate with thickness $d=1$ mm. Before we can finally specify the values of the circuit elements in the network, we must appropriately choose the number and the thickness of the layers, and the number of unit cells in each layer. The long-wavelength approximation should be well satisfied so that each unit cell can successfully mimic the locally homogeneous and anisotropic medium in the small trapezoid like region. In our design, 15 concentric layers of L-C MTMs are used to realize the cloak shell and another 15 layers to describe the background medium. Each layer is equally divided into 90 unit cells along the angular direction, resulting in 4° span angle for each unit cell. Based on Eqs. (6) and (7), the circuit parameters of the cloak and the background medium can be calculated. Then, chip inductors and capacitors with available values most close to the calculated ones are chosen to realize the network. The theoretical (blue solid line) and the experimental (red dotted line) values of the lump elements are shown in Fig. 3. Since the whole structure is rotationally symmetrical, we only need to give dependence of the circuit parameters on the radius. The whole experiment device measures about 400 mm $\times$ 400 mm $\times$ 1 mm and is shown in Fig. 4. Also shown in the inset is a magnification of a single unit cell, consisting of four surface-mounted inductors in series and one capacitor in shunt to the ground by a via-hole, similar to the schematic in Fig. 1. The performance of such a device under stable states

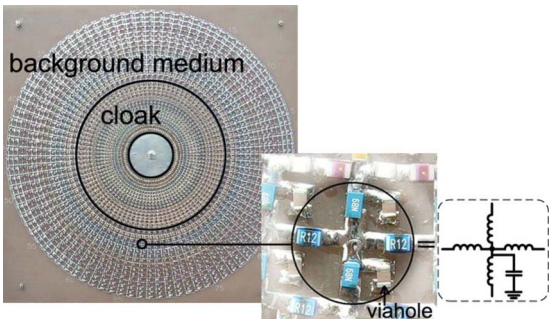

FIG. 4. (Color online) The photograph of the fabricated cloak with background medium for experiment. The inset is a magnification of a single unit cell, consisting of four surface-mounted inductors in series and one capacitor in shunt to the ground by a via-hole, similar to the schematic in Fig. 1.

has been studied.[23] In realistic applications, the dynamic responses of a cloak to a wideband time-domain signal is ultra important. In the following section, the response of the device to a broadband EM pulse will be investigated experimentally.

III. EXPERIMENT ON THE RESPONSE OF THE CLOAK TO A WIDEBAND EM PULSE

In the frequency band below 40 MHz (the design frequency), the long-wavelength limit is well satisfied and the chip components (the inductors and the capacitors) have nonresonant nature. In this case, μ_r, μ_θ, and ε_z in each unit cell are directly proportional to L_θ, L_r, and C_z whose values change gradually as the frequency changes. Hence, the fabricated cloak device has medium parameters with low dispersion in the band below 40 MHz, and is expected to exhibit broadband characteristics. To demonstrate the performance of the cloak, an Agilent E5071C vector network analyzer (VNA) was employed to take transmission scattering parameter measurements. Port 1 of the VNA provides the excitation via a coaxial feed, with its outer conductor mounted onto the ground plane at the backside of the FR4 substrate, and its center pin extending through a hole in the substrate and soldered to the center of a unit cell as the expiation point. Hence, a point source is introduced to excite a cylindrical wave. Port 2 of the VNA provides a near-field coaxial probe that can scan over the surface of the cloak shell and the background region. A broadband amplifier with high input impedance is designed and connected between the probe and port 2 of the VNA to amplify the signal and to reduce the disturbance of the voltage distribution when the probe touches the node during measurement. In the experiment, the inductors L_r at the inner boundary of the cloak are grounded to create an effect of a PEC boundary.

To obtain the transient response of the cloak to a wideband pulse with VNA, two approaches can be chosen. The first approach is transforming the frequency domain response based on frequency sweeping measurement to the time-domain response by computing the Inverse Fourier Transform (IFT) by ourselves. The second approach is using the time-domain analysis function of the VNA, in which the IFT

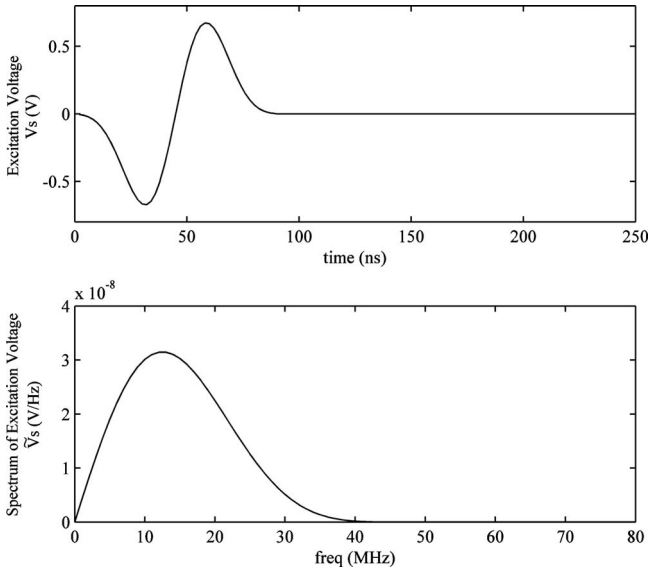

FIG. 5. The excitation voltage and its spectrum

is performed by the integrated data processor of VNA to automatically give the time-domain response. In the experiment, we choose the first approach and benefit it from its flexibility in the form of excitation voltage pulse. The excitation point was set in the background region with location $x_s=0$ cm, $y_s=17.4$ cm. Here, the original point (0, 0) was set at the center of the cloak. The first derivative of a Blackmann-Harris (BH) pulse[30] was chosen as the excitation voltage that vanishes completely after time $T_c=90$ ns with following expression:

$$V(x_s,y_s,t) = -a_1 \sin\left(2\pi\frac{t}{T_c}\right) + 2a_2 \sin\left(2\pi\frac{2t}{T_c}\right) - 3a_3 \sin\left(2\pi\frac{3t}{T_c}\right), \quad (8)$$

where $a_1=0.48829$, $a_2=0.14128$, $a_3=0.01168$. The cutoff frequency of the pulse is about $f_c=3.6/T_c=40$ MHz. The wave form of the excitation voltage in the time-domain $V(x_s,y_s,t)$ and its spectrum $\tilde{V}(x_s,y_s,f)$ are shown in Fig. 5.

After the frequency sweeping measurement of each node with a 2D spatial scanning of the cloak shell and background region, the transmission coefficients between the excitation voltage at the feeding point (x_s,y_s) and response voltage at any node (x,y) can be extracted in the frequency domain,

$$\tilde{T}(x,y,f) = \frac{\tilde{S}_{21}(x,y,f)}{\tilde{S}_{21}(x_s,y_s,f)}, \quad (9)$$

where $\tilde{S}_{21}(x,y,f)$ is the measured transmission scattering parameter from Port1 to Port2 of VNA at node (x,y) and frequency f. Then, the transient voltage response at any node (x, y) can be obtained in the time domain based on following IFFT:

$$V(x,y,t) = IFFT[\tilde{V}(x_s,y_s,f)\tilde{T}(x,y,f)] \quad (10)$$

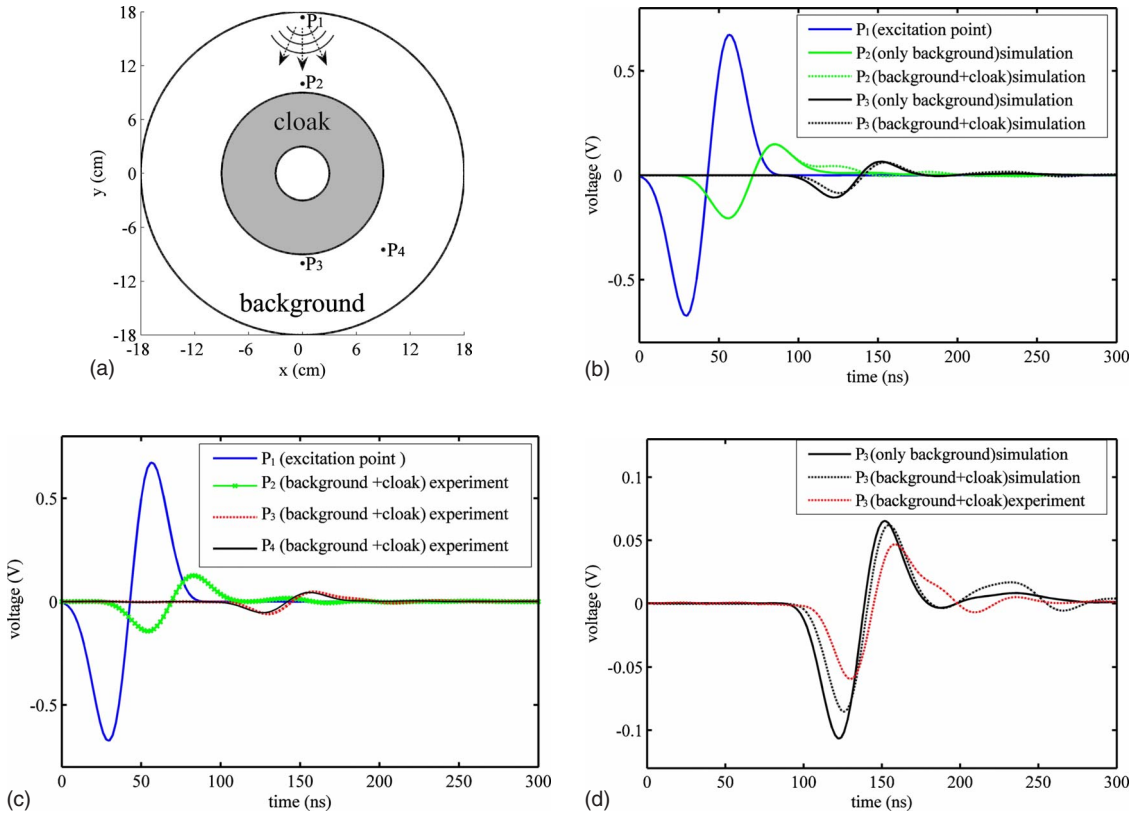

FIG. 6. (Color online) Transient voltages at four points P_1, P_2, P_3, and P_4. (a) The location of the four points in the background. (b) The simulation results of the transient voltages at P_1, P_2, P_3. (The blue line is the excitation voltage at P_1. The green solid line and black solid line are the voltages at P_2 and P_3 for only the background without cloak and metallic cylinder. The green dotted line and the black dotted line are the voltages at P_2 and P_3 for the background with cloaked metallic cylinder.) (c) The experimental results of the transient voltages at P_1, P_2, P_3, and P_4 for the background with cloaked metallic cylinder. (d) Comparison of the simulated and the measured voltages at P_3. (The black solid line is the simulation result for only the background without cloak and metallic cylinder. The black dotted line and the red dotted line are the simulated and measured voltages for the background with cloaked metallic cylinder.)

It is has been predicted by theoretical and numerical methods[15–17] that the dispersion of the cloak may lead to two effects when a pulse is passing through a cloak shell. The first effect is the time delay which becomes stronger near the inner boundary of the cloak. Another effect is the pulse broadening effect resulted from the different phase and energy velocities in different frequencies. These two effects may finally results in the spatial distortion of the beam shape. To study these effects of our cloak, the transient voltages at the excitation point $P_1(0\ \text{cm}, 17.4\ \text{cm})$ and other three points $P_2(0\ \text{cm}, 10\ \text{cm})$, $P_3(0\ \text{cm}, -10\ \text{cm})$, $P_4(9\ \text{cm}, -8.48\ \text{cm})$ are investigated (as shown in Fig. 6). The points P_2 and P_3 are both located along the center line of the cloak, while P_2 in front of the cloak and P_3 behind the cloak. P_4 and P_3 have same distance to P_1, while P_4 is located away from the center line of the cloak.

Figure 6(b) shows the simulated voltages at P_2, P_3, when P_1 is excited by the same voltage as in the experiment. The solid lines in Fig. 6(a) are the voltages for only the background medium without the cloak and the metallic cylinder, while the dotted lines are for the background medium with cloak and the metallic cylinder. It is seen that, the changes for the time delay and the shape of the pulses at P_3 is little when the cloaked metallic cylinder is embedded into the background. In the simulation, loss of the inductor and capacitor has not been taken into account.

The measured pulses at P_2, P_3, P_4 for the fabricated cloak device are shown in Fig. 6(c). It can be found that the measured time delay between P_2 and P_3 for the wave propagating in the background medium with cloak and metallic cylinder is about 73 ns. It is also found from Fig. 6(b) that the simulated time delay between P_2 and P_3 for the wave propagating in the background medium without cloak and metallic cylinder is 67 ns. Based on the simulation and the experiment results, Table I lists the arrival moments, which are defined as the time when the positive peak of a pulse arrives, for more clear comparison. It can be further found from Fig. 6(c) that the time durations and the shapes of the measured pulses at different points are almost same. The small time delay and pulse broadening effect of our cloak resulted from the low dispersion of the unit cell structure, which leads to the broadband property of the cloak.

In Fig. 6(d), the pulses at P_3 for three different cases are replotted for more clear comparison. The black solid line is the simulation result for only the background without cloak and metallic cylinder. The black dotted and the red dotted lines are the simulated and measured results for the background with cloaked metallic cylinder. It is seen that, the

TABLE I. The arrival moments of the pulses at different points.

	Arrival moments of the pulse (ns)		
Different points	Simulation for only background	Simulation for background with cloak and metallic cylinder	Experiment for background with cloak and metallic cylinder
P_1	30	30	30
P_2	56	56	57
P_3	123	126	130
P_4	123	124	126

measured pulse has smaller amplitude than the simulated pulse under the same case. This results from the loss of the inductors and the capacitors in the experiment.

Based on the simulation results, we can also calculate the scattered energy of the uncloaked metallic cylinder W_{unc} and the cloaked one W_c when excited by a same voltage pulse at P_1. First, the scattered voltage pulses at each node can be obtained by subtracting the incident field (the voltage distribution for background medium without cloak and metallic cylinder) from the total field. Then, the scattered energy at i$^{\text{th}}$ node in the background medium can be calculated based on following integration:

$$W(i) = \int V_s(i,t) I_{\text{sout}}(i,t) dt \tag{11}$$

where $V_s(i,t)$ and $I_{\text{sout}}(i,t)$ are the scattered transient voltage and the outward current at i$^{\text{th}}$ node. The integration is performed over the whole duration time. In Fig. 7, the scattered energy distribution dependent on the scattering angle θ_s along a sampling circle with radius $r_s=15.3$ cm is shown. Here, the positive y direction is defined as $\theta_s=0$ for symmetry of the curve. The blue line is for the cloaked metallic cylinder, while the red dotted line is for the bared metallic cylinder. It is found that, the cloak device greatly reduce the scattered energy in different scattering angles. The maximum scattered energy distribution and the total scattered energy are both reduced more than 10 times. A more interesting phenomenon is that the scatted energy of the cloaked structure is almost isotropy over all the angles.

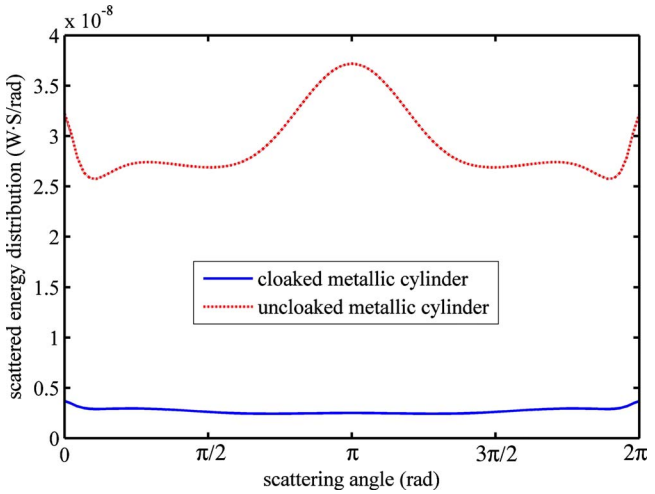

FIG. 7. (Color online) The simulated scattered energy distribution along a sampling circle with radius $r_s=15.3$ cm. The blue solid line is for the cloaked metallic cylinder. The red dotted line is for the uncloaked metallic cylinder. Here, the scattering angle θ_s is defined as $\theta_s=0(+y)$, $\theta_s=\pi/2(-x)$, $\theta_s=\pi(-y)$, $\theta_s=3\pi/2(+x)$.

Finally, the dynamics of pulse propagation across the cloak device is measured. Figure 8 depicts nine time snapshots of the voltage distribution based on the experimental results. A movie (media 1) is also provided as the supplemental online material.[31] As the wavefront entering the cloak, the center part of the beam begins to compress. After the wavefront reaches the inner boundary, it separates to pass around the metallic cylinder and then well recomposed on the opposite side behind the cloak. As the wave leaving the cloak shell, the circular wavefront of the cylindrical wave is restored without obvious spatial distortion. However, the scattering of the cloaked metallic cylinder and the attenuation of the wave along the propagation path can still be observed. The imperfection of the cloak performance is relevant to complex factors, including the singularity of the parameters at the inner boundary which cannot be dealt with ideally in the experiment, the relatively large tolerance (about 15%) and low quality factors (about 20) of the inductor elements, the loss introduced by the dielectric substrate, and the imperfect manual welding process. It is necessary to point out that, the blur of the beam near the outer boundary of the background is mainly due to the nonideal match absorption of the Bloch impedance. This phenomena is not relevant to the cloak performance and will not exist when the cloak is practically used in infinitely extended background medium.

It should also be noted that, a broadband cloak with good performance is required to support group velocities greater than the wave velocity in the background medium. Since the group velocity inside a cloak cannot exceed the group velocity in the air, a nice broadband solution is theoretically impossible when the background medium is air. Even though, for air background, cloak devices realized with nonresonant and low-dispersive unit cells could exhibit better broadband performance than those realized with resonant and strong-dispersive unit cells.

The results and the discussions in this section show that, it is possible to design a cloak device with broadband characteristic for background medium having wave velocity slower than that in the air, such as to cloak an object in the earth or in the multilayered medium.

IV. CONCLUSIONS

In this paper, the response of the cylindrical cloak to a broadband EM pulse was investigated with experiment. The transformation medium of the cloak devices was realized with full parameters based on a nonuniform L-C network in which the three branches of unit cells were employed to in-

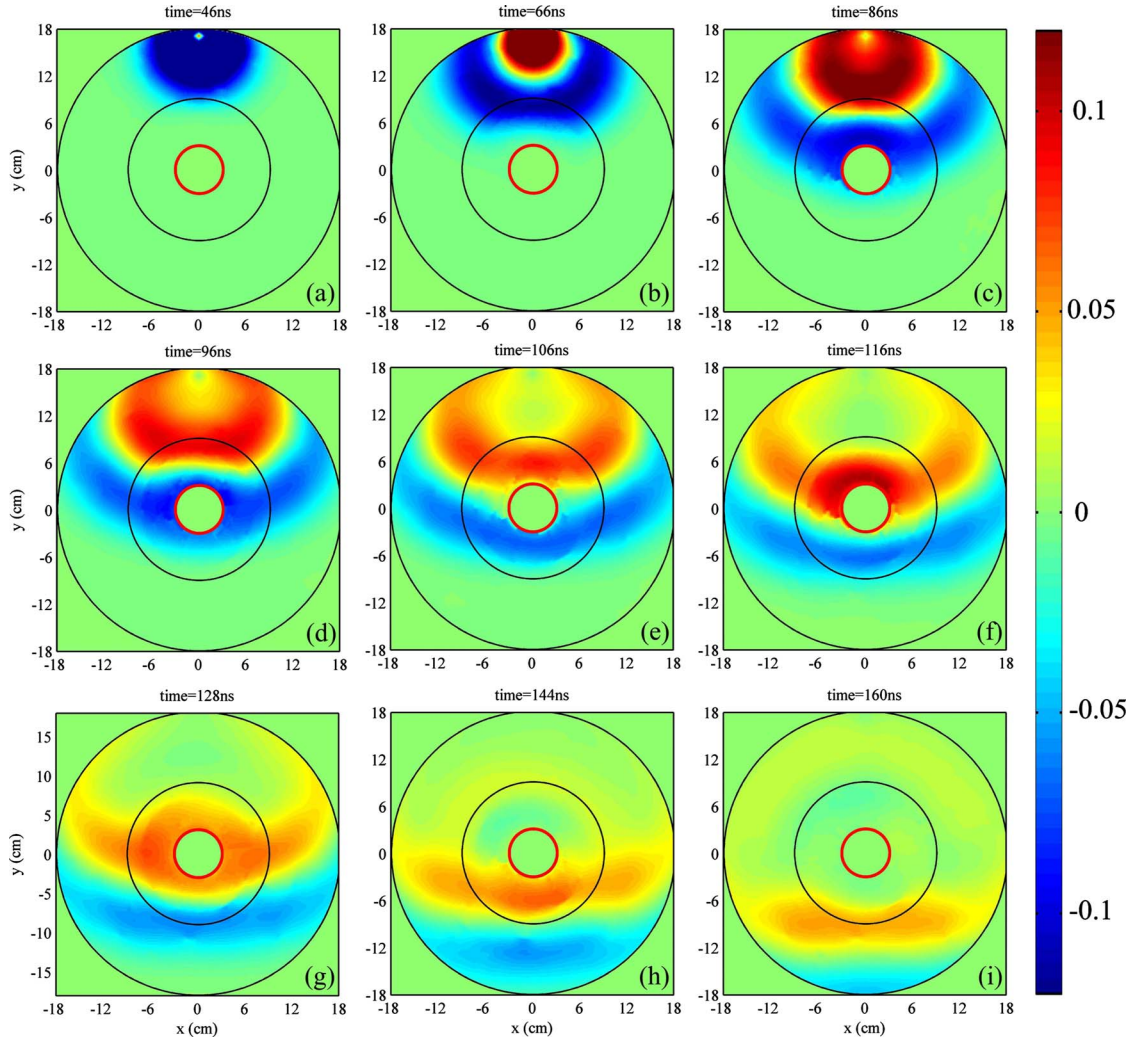

FIG. 8. (Color online) Nine time snapshots of the measured voltage distribution (Media 1). (a) $t=46$ ns, (b) $t=66$ ns, (c) $t=86$ ns, (d) $t=96$ ns, (e) $t=106$ ns, (f) $t=116$ ns, (g) $t=128$ ns, (h) $t=144$ ns, (i) $t=160$ ns.

dependently control the material parameters μ_r, μ_θ, and ε_z, respectively. The time delay effect, the pulse broadening effect and the scattered energy reduction ability of the cloak were investigated based on the experiment and simulation results. The dynamics of pulse propagation across the cloak device was measured. It is found that the nonresonant nature of the unit cell structures leads to a very low dispersion of the cloak parameters and results in the invisibility of the cloak to the broadband EM pulse. More practical applications may be brought by the broadband property of the proposed cloak.

ACKNOWLEDGMENTS

This work was supported by the National Natural Science Foundation of China (Grants No. 60990323 and No. 60990320), and the Knowledge Innovation Program of Chinese Academy of Sciences.

[1] A. Alù and N. Engheta, Opt. Express **15**, 3318 (2007).
[2] A. Alù and N. Engheta, Phys. Rev. Lett. **100**, 113901 (2008).
[3] G. W. Milton and N. A. Nicorovici, Proc. R. Soc. London, Ser. A **462**, 3027 (2006).
[4] N. A. Nicorovici, G. W. Milton, R. C. Mcphedran, and L. C. Botten, Opt. Express **15**, 6314 (2007).
[5] J. B. Pendry, D. Schurig, and D. R. Smith, Science **312**, 1780 (2006).
[6] D. Schurig, J. J. Mock, B. J. Justice, S. A. Cummer, J. B. Pendry, A. F. Starr, and D. R. Smith, Science **314**, 977 (2006).
[7] D. Schurig, J. B. Pendry, and D. R. Smith, Opt. Express **14**, 9794 (2006).
[8] S. A. Cummer, B.-I. Popa, D. Schurig, David R. Smith, and John Pendry, Phys. Rev. E **74**, 036621 (2006).

[9] Z. Ruan, M. Yan, C. W. Neff, and M. Qiu, Phys. Rev. Lett. **99**, 113903 (2007).
[10] H. Y. Chen, Z. X. Liang, P. J. Yao, X. Y. Jiang, H. Ma, and C. T. Chan, Phys. Rev. B **76**, 241104 (2007).
[11] B. L. Zhang, H. S. Chen, B.-I. Wu, Y. Luo, L. X. Ran, and J. A. Kong, Phys. Rev. B **76**, 121101 (2007).
[12] C. Li and F. Li, Opt. Express **16**, 13414 (2008).
[13] D. H. Kwon and D. H. Werner, Appl. Phys. Lett. **92**, 013505 (2008).
[14] C. Li, K. Yao, and F. Li, Opt. Express **16**, 19366 (2008).
[15] H. Chen and C. T. Chan, J. Appl. Phys. **104**, 033113 (2008).
[16] Y. Zhao and Y. Hao, J. Comput. Phys. **228**, 7300 (2009).
[17] B. L. Zhang, B.-I. Wu, and H. S. Chen, Opt. Express **17**, 6721 (2009).
[18] I. I. Smolyaninov, Y. J. Hung, and C. C. Davis, Opt. Lett. **33**, 1342 (2008).
[19] R. Liu, C. Ji, J. Mock, J. Y. Chin, T. J. Cui, and D. R. Smith, Science **323**, 366 (2009).
[20] J. Valentine, J. Li, T. Zentgraf, G. Bartal, and X. Zhang, Nature Mater. **8**, 568 (2009).
[21] P. Alitalo, F. Bongard, J.- F. Zurcher, J. Mosig, S. Tretyakov, Appl. Phys. Lett. **94**, 014103 (2009).
[22] X. Liu, C. Li, K. Yao, X. K. Meng, and F. Li, IEEE Antennas Wireless Propag. Lett. **8**, 1154 (2009).
[23] X. Liu, C. Li, K. Yao, X. K. Meng, W. Feng, B. H. Wu, and F. Li, Appl. Phys. Lett. **95**, 191107 (2009).
[24] G. V. Eleftheriades, A. K. Iyer, and P. C. Kremer, IEEE Trans. Microwave Theory Tech. **50**, 2702 (2002).
[25] C. Caloz and T. Itoh, IEEE Trans. Antennas Propag. **52**, 1159 (2004).
[26] A. Grbic and G. V. Eleftheriades, IEEE Trans. Microwave Theory Tech. **51**, 2297 (2003).
[27] A. Grbic and G. V. Eleftheriades, Phys. Rev. Lett. **92**, 117403 (2004).
[28] K. G. Balmain, A. A. E. Luttgen, and P. C. Kremer, IEEE Trans. Antennas Propag. **51**, 2612 (2003).
[29] A. Grbic and G. V. Eleftheriades, IEEE Trans. Antennas Propag. **51**, 2604 (2003).
[30] F. J. Harris, Proc. IEEE **66**, 51 (1978).
[31] See supplementary material at http://link.aps.org/supplemental/10.1103/PhysRevB.81.115133 to further visualize the dynamic process.